



CHORUS

This is the accepted manuscript made available via CHORUS. The article has been published as:

In situ x-ray scattering study of Ag island growth on Si(111)7×7

Yiyao Chen, M. W. Gramlich, S. T. Hayden, and P. F. Miceli

Phys. Rev. B **94**, 045437 — Published 28 July 2016

DOI: [10.1103/PhysRevB.94.045437](https://doi.org/10.1103/PhysRevB.94.045437)

In situ X-ray Scattering Study of Ag Island Growth on Si(111)7x7

Yiyao Chen, M. W. Gramlich, S. T. Hayden, and P. F. Miceli*

Department of Physics and Astronomy, University of Missouri, Columbia, Missouri 65211, USA

(Dated: July 13, 2016)

We report on the epitaxial relationship between Ag and the Si(111)7x7 substrate where the wetting layer and the emergence of islands was investigated using in situ x-ray scattering with a combination of grazing incidence diffraction, specular reflectivity and crystal truncation rod measurements. The atomic-scale structure of the wetting layer evolves continuously with coverage until a transition where it ceases to change its structure concomitantly with the appearance of islands. The islands are observed to reside on the Si(111)7x7 and, although the minimum average island height is three atomic layers of face-centered cubic Ag, the average island height depends on the coverage and temperature. The majority of the Ag islands are oriented along the symmetry-equivalent Si crystallographic axes and a minority population of islands are rotated by 15.7° . A coincidence-site lattice model is used to show that kinetic considerations lead to the observed island orientations.

PACS numbers: 61.05.cm, 61.46.Hk, 68.55.J-, 68.35.Ct

I. INTRODUCTION

Metals grown on semiconductor surfaces represent a broad class of materials systems that play a ubiquitous role in both conventional and emerging technologies involving Schottky barriers and novel nanoscale electrical and optical devices¹⁻³. Despite their ubiquity, metal/semiconductor interfaces present significant challenges to a fundamental understanding of their growth and formation, even for simple elemental metals. Early work on the growth of Ag on GaAs⁴ demonstrated the ability of metals to form unexpectedly flat surfaces – an effect driven by the conduction electrons in the metals^{5,6}. Moreover, nanoscale metals, such as thin islands produced during epitaxial growth, can exhibit quantum size effects (QSE) where the conduction electrons are significantly influenced by quantum confinement⁷. The energy levels from such QSE can, in turn, influence the growth and stability of metallic islands grown on semiconductor surfaces⁸⁻¹⁰. This effect is dramatically manifested in the growth of Pb on Si(111) where an oscillatory bi-atomic layer stability of island heights (“magic heights”) is observed^{11,12} early in the growth and there is a novel non-classical coarsening exhibited by the islands in the later stages of the island evolution¹³. Similar oscillatory growth has been recently observed for In on Si(111)¹⁴.

As it is a noble metal, there has been extensive interest to understand the growth of Ag on Si(111)7x7. At low coverage, half unit cells (HUC) of the Si(111)7x7 form a template for the nucleation of small Ag clusters that coalesce into a wetting layer consisting of a discontinuous network of Ag¹⁵⁻²⁰. At higher coverage, around 0.4 ML, studies suggested that islands begin to form *on top* of this wetting layer, although, little is known about the crystallographic structure of the wetting layer or how the islands interface with it. Gavioli et al. observed that

Ag islands grow with flat tops on Si(111)7x7 and the islands exhibit a minimum height of two monolayers *above* the wetting layer²¹; that is, there can be two layers or more, but there is no oscillatory stability as in the case of Pb. This behavior has been observed by a number of groups²²⁻²⁵, although, it has been difficult to connect the observed minimum height to QSE. Recently, however, in situ x-ray scattering experiments by our group (Chen et al.²⁶) revealed that the minimum island height can be understood from the known electronic structure of atomically thin Ag. Moreover, those experiments showed that the minimum island height is three atomic layers of face-centered cubic (FCC) Ag in direct contact with the substrate, rather than a bilayer on top of a wetting layer having 7x7 symmetry.

Despite a body of work largely performed by scanning-tunneling microscopy (STM) on Ag/Si(111)7x7 that looks at the early stages of growth¹⁵⁻²⁰ and the island morphology²¹⁻²⁵, little is known about the atomic scale structure and the epitaxy involved in the transition from the Ag wetting layer to the islands. The discontinuous nature of the wetting layer is unusual and it is not known how it evolves during the growth of the islands. Also, the structural relationship of the islands with respect to the substrate and reconstructed surface has not been carefully explored.

In this paper, we present the results of our in situ x-ray scattering investigation of the epitaxial relations for Ag grown on Si(111)7x7. Using measurements of surface diffraction from the 7x7 interface, specular reflectivity and crystal truncation rods, essential new information about the epitaxial relationship between the wetting layer, the islands and the substrate is obtained. The atomic-scale structure of the wetting layer is found to evolve continuously up until a saturation coverage, at which point the discontinuous wetting layer no longer adds Ag or changes its structure. The results suggest a *macroscopic* two-phase coexistence of the islands with the wetting layer. We investigate the evolution of the islands, which are found to reside on a modified Si(111)7x7,

*e-mail: micelip@missouri.edu

and they exhibit an average height that is both coverage and temperature dependent above the three-layer minimum height. A detailed model is presented that allows the determination of the island height distributions from the specular reflectivity and the crystal truncation rods. Two island orientations are observed and both are examined in the context of a coincidence-site lattice model based on the FCC Ag interface with Si(111)7x7. It is argued that the observed orientations arise because of clustering that facilitates the nucleation of islands.

II. EXPERIMENTAL DETAILS

X-ray scattering experiments were performed in situ using the surface scattering chamber (base pressure of 1×10^{-10} Torr) on a PSI diffractometer located at the 6IDC beam line at the Advanced Photon Source using a photon energy of 16.2keV. The reciprocal lattice will be described by hexagonal coordinates $(H,K,L)_H$ for Si, which is defined by the following relationship between hexagonal and cubic coordinates: $a_H = a/\sqrt{2}$ and $c_H = \sqrt{3}a$, where $a = 5.431\text{\AA}$ is taken as the room temperature Si cubic lattice constant. Using an H subscript to indicate hexagonal coordinates and no subscript for cubic coordinates, we have $[0,0,3]_H = [1,1,1]$ along the surface normal direction, $[3,0,0]_H = [4,2,2]$ and $[0,3,0]_H = [\bar{2},\bar{2},4]$. Ag reciprocal lattice coordinates will be designated as $\text{Ag}(H,K,L)_H$ where the cubic Ag lattice constant is taken to be 4.090\AA . For example, $\text{Ag}(1,1,0)_H = (1.328,1.328,0)_H$.

The commercially-available 1mm-thick n-type Si(111) substrates used in these studies had a resistivity in the range of 1-10 Ω cm. Surface miscut angles were determined by x-ray reflectivity to be between 0.015° - 0.05° . The Si(111)7x7 surface was prepared by heating the Si(111) substrate to 1200°C for ~ 1 min and then slowly cooling from 1000°C for over 10 min to obtain the reconstructed surface. The quality of the surface was determined by transversely scanning the $(8/7, 0, 0.1)_H$ in-plane reflection. It exhibited an angular width of 0.02° to 0.05° , which corresponds to domain sizes between 8000\AA and 3300\AA . This large domain size, which is on the order of the step length given by the surface miscut angle, was routinely observed for all surfaces that were prepared as described above.

Ag was deposited on the clean Si(111)7x7 surface at a given fixed temperature between 260K and 400K using a thermal evaporator with a deposition rate of $\sim 1.1 \text{ ML} \pm 0.1 \text{ ML/min}$, where 1 ML is one monolayer of Ag(111) ($1 \text{ ML} = 1.38 \times 10^{15} \text{ atoms/cm}^2$). It is noted that a two-step process with annealing after low-temperature deposition had been used in early work²¹ whereas later studies showed that similar results could be obtained in a single step with deposition near room temperature without annealing²²⁻²⁵. Here, we use the single-step deposition. The deposition rate was determined by a commercial quartz crystal oscillator that was calibrated from

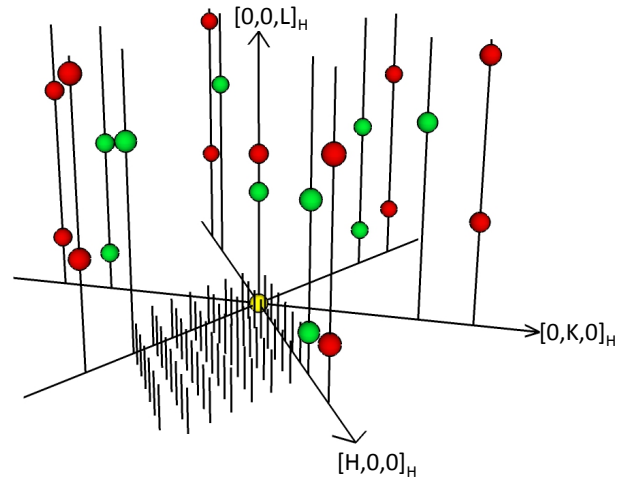


FIG. 1: Schematic diagram illustrating the crystal truncation rods for Ag/Si(111)7x7, where the surface normal is along $[0,0,L]_H$. Bragg points are represented by green (light) spheres for Si and red (dark) spheres for Ag, from $L=0$ to $L=7$. The specular reflectivity is along $[0,0,L]_H$ whereas the truncation rods for the Si lattice and the incommensurate Ag lattice correspond to rods having non-zero H and/or K . A small subset of the fractional rods from the 7x7 wetting layer, which have no Bragg points, are shown schematically in the region between $[H,0,0]_H$ and $[H,\bar{K},0]_H$.

the period of x-ray intensity oscillations measured at the Ag specular anti-Bragg position during the layer-by-layer growth of Ag/Ag(001). The sample was cooled using a He closed-cycle refrigerator while heating employed a tungsten filament behind the sample. Heating for the purpose of preparing the Si(111)7x7 was performed by electron bombardment whereas maintaining the temperature during the scattering measurements utilized radiative heating from the tungsten filament. The temperature was measured by a type K thermocouple connected to the bottom of the sample holder, which was also used for temperature control with a feedback system. The temperature stability was $\pm 0.5^\circ\text{C}$ and the absolute temperature accuracy was better than $\pm 10^\circ\text{C}$.

Three types of x-ray scattering measurements were performed: specular reflectivity, crystal truncation rods and grazing incidence diffraction from fractional-order rods. The relative contribution of scattering from the Si substrate, the Ag/Si(111)7x7 reconstructed surface and the FCC Ag islands will depend on where the measurements are performed in reciprocal space, as shown schematically in Fig. 1. The light and dark spheres represent Bragg points from bulk Si and Ag, respectively, and they are elongated into crystal truncation rods (CTR) along the direction perpendicular to the surface, as indicated by the vertical lines. Because the Ag islands and Si are incommensurate, their respective rods do not overlap except for the specular rod for which $H=K=0$. Therefore, scans performed along the FCC Ag rods will independently reveal the morphology of the Ag islands. Specular

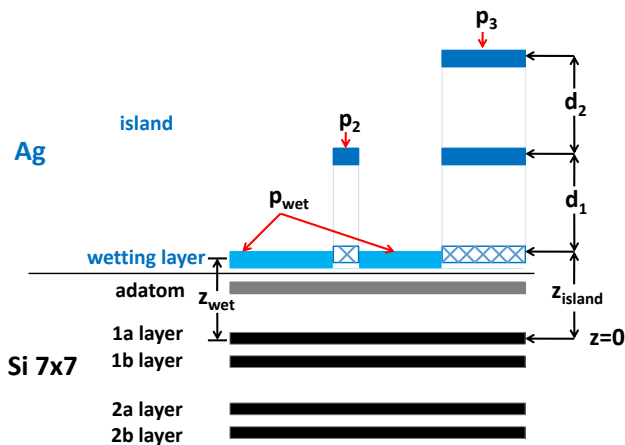


FIG. 2: Side view showing the atomic layers used in the structural model for specular reflectivity and crystal truncation rods. The Ag wetting layer and Ag islands sit on the Si(111)7x7 structure; the bulk Si substrate is not shown. p_j is the fraction of the surface occupied by islands having a height j . The bottom atomic layer of the islands are cross-hatched to indicate that its structure is investigated.

reflection, however, which is measured along $[0,0,L]_H$, is a unique CTR where the scattered amplitude from all atomic layers of the substrate and the film will interfere and contribute to the specular rod. The third type of measurement is grazing incidence diffraction, with $L \sim 0$, from the fractional-order rods that arise from the interfacial layer having the 7x7 symmetry.

III. MODEL FOR THE SPECULAR REFLECTIVITY AND THE CRYSTAL TRUNCATION RODS

Before proceeding, we discuss the model that is used to analyze and interpret both crystal truncation rod and x-ray reflectivity measurements. This model was used in the work of Chen et al.²⁶, but the details and derivation were not discussed there.

A schematic side-view of the atomic layers in the model is shown in Fig. 2. Note that it is only necessary to draw the vertical structure of the atomic layers because a specular reflectivity measurement is sensitive to all of the atomic layers in the sample regardless of their lateral structure, whereas a crystal truncation rod measurement will detect only the atomic layers in Fig. 2 that have the in-plane symmetry of the rod being measured. In particular, we investigate the rods that have the in-plane Ag FCC structure.

The structural model assumes a semi-infinite bulk Si(111) substrate having a Si(111)7x7 reconstructed surface, which consists of five Si layers: 2b, 2a, 1b, 1a and the ad-atom layer. Its structure has been described by Robinson et al.²⁷ and we utilize the atomic layer posi-

tions and occupancies from that work. The Ag wetting layer and the Ag islands sit on top of the Si(111)7x7 at a distance z_{wet} and z_{island} , respectively, measured relative to the Si-1a layer. Because the structure of the first atomic layer in the island remains a central question, it is drawn as cross-hatched: its relationship to the wetting layer and the islands will be explored in these experiments. The spacings between the Ag atomic layers in the islands are given as d_n and the fraction of the surface occupied by islands of height j is given by p_j , which describes the island height distribution. p_0 is the fraction of the surface that has bare Si(111)7x7, p_{wet} is the fraction of the surface covered by the wetting layer, p_1 is the surface fraction of a single-layer island, p_2 is the fraction of the surface that contains 2-layer islands, and etc. By definition all surface fractions add to unity, $p_{wet} + \sum_{j=0}^{\infty} p_j = 1$, which imposes a constraint on the values of the p 's.

The scattered x-ray intensity is proportional to the square of the total amplitude scattered from the Ag film and the Si substrate, which is given by the differential scattering cross section, $\frac{d\sigma}{d\Omega} = |A|^2 |V_{sub}|^2$. The total amplitude A can be expressed as

$$A = \rho_{Si} f_{Si} A_{Si} + \rho_{Ag} f_{Ag} A_{Ag} \quad (1)$$

where f_{Si} and f_{Ag} are the atomic form factors that also include the thermal Debye-Waller factor e^{-M} for Si and Ag, respectively. M is calculated²⁸ from the Debye temperature, which is taken to be 225K for Ag and 645K for Si. ρ_{Ag} and ρ_{Si} are the bulk areal densities of the Ag(111) and Si(111) planes; $\rho_{Ag} = 1.763\rho_{Si}$ is used here. The factor $|V_{sub}|^2$ is due to the substrate roughness and it is expressed as²⁹

$$|V_{sub}|^2 = e^{-4 \frac{\sigma_{sub}^2}{d_{Si}^2} \sin^2 \frac{Q d_{Si}}{2}} \quad (2)$$

where $Q = \frac{2\pi L}{c_H}$, $d_{Si} = \frac{c_H}{3}$ is the Si(111) layer spacing, and σ_{sub} is the root-mean-square (RMS) roughness of the Si substrate.

The Si amplitude has contributions from both the bulk Si and from the Si(111)7x7 reconstructed surface, $A_{Si} = A_{Si}^{bulk} + A_{Si}^{DAS}$, where A_{Si}^{DAS} is given by the dimer-adatom stacking fault (DAS) model³⁰ of the reconstructed surface according to

$$A_{Si}^{DAS} = \sum_j \eta_j e^{iQz_j} e^{-\frac{1}{2}Q^2\zeta_j^2} \quad (3)$$

where j sums over the five layers (2b, 2a, 1b, 1a and adatom layer for $j=1$ to 5) of the DAS model with each layer having a position z_j , a layer position fluctuation ζ_j , and a layer occupancy η_j .²⁷ A_{Si}^{bulk} describes the amplitude from the semi-infinite bulk Si,

$$A_{Si}^{bulk} = \frac{\left(1 + e^{-\frac{\pi i L}{6}}\right) \left(1 + e^{-\frac{2\pi i L}{3}} + e^{-\frac{4\pi i L}{3}}\right)}{1 - e^{-2\pi i L}} e^{-iQz_{3a}} \quad (4)$$

where $z = 0$ is located at the Si-1a layer so that z_{3a} is the starting position of the bulk Si below the reconstruction.

When Ag is first deposited, it commensurately wets the Si(111)7x7 up to an areal density of the saturation coverage ϕ_{wet} (~ 0.4 ML, determined below), measured relative to a Ag(111) plane ($\equiv 1$). Generally, we can also allow the model to express the areal density, ϕ_n , of the Ag atomic layers in the islands. Although $\phi_n = 1$ for the FCC layers in the island, ϕ_1 remains a question, as indicated by the cross-hatched first layer in Fig. 2: $\phi_1 = \phi_{wet}$ if the islands grow on top of the wetting layer whereas

$\phi_1 = 1$ if the islands are FCC Ag all the way to the substrate. With these considerations, the Ag coverage is given as

$$\Theta = p_{wet}\phi_{wet} + \sum_{j=1} p_j \sum_{n=1}^j \phi_n \quad (5)$$

and the Ag specular scattering amplitude from all of the Ag layers is given as

$$A_{Ag} = p_{wet}\phi_{wet}e^{iQz_{wet}}e^{-\frac{1}{2}Q^2\sigma_{wet}^2} + \sum_{j=1} p_j \sum_{n=1}^j \phi_n e^{iQz_n}e^{-\frac{1}{2}Q^2\sigma_j^2} \quad (6)$$

where the second term in both equations is due to the FCC Ag islands and $z_n = z_{island} + d_1 + d_2 + \dots + d_{n-1}$. If all Ag interatomic layer spacings are the same, then $z_n = z_{island} + (n-1)d_{Ag}$. For bulk Ag, we take $d_{Ag} = 2.361\text{\AA}$. σ_{wet} and σ_j are the RMS variation in the vertical position of the wetting layer and the j -layer island, respectively. We will take $\sigma_j = \sigma$ to be the same for all islands. Because our studies find (see below) $z_{wet} \approx z_{island}$ and because specular reflection does not distinguish the Ag 7x7 structure from Ag FCC, p_1 will effectively be indistinguishable from p_{wet} in the specular reflectivity measurements so that p_{wet} will include p_1 in this case.

In contrast to the specular reflectivity, the scattering amplitude for a FCC Ag truncation rod has no contribution from the Si substrate or from the Ag wetting layer because these do not have the Ag FCC structure. Moreover, the cross-hatched region in the first atomic layer of the islands in Fig. 2 will contribute to the rod only if that layer exhibits the FCC structure of Ag. We therefore take $\phi_1 = 1$. The scattering amplitude for a FCC Ag(H,K)_H truncation rod is given as

$$A_{Ag} = \sum_{j=1} p_j \sum_{n=1}^j (e^{2\pi i \frac{2H+K}{3}})^{n-1} e^{iQz_n} e^{-\frac{1}{2}Q^2\sigma_j^2} \quad (7)$$

where H and K here refer to the Miller indices appropriate to bulk Ag in hexagonal coordinates. It is noted that p_j determined from the measurement of truncation rods will have an overall unknown scale factor whereas p_j can be determined on an absolute scale from specular reflectivity because it includes a strong reference amplitude from the substrate.

To compare the model with the measurements, several geometrical corrections must be applied^{31,32}. We define the incident angle as α_i , the exit angle, α_f , and the in-plane scattering angle, Φ . For specular reflection, $\alpha_i = \alpha_f = \theta$, $\Phi = 0$, and we multiply the model for the

differential cross section by the following factors: $1/Q^2$ for the Lorentz factor and active area correction, the linear polarization correction $\cos^2(2\theta)$, and a foot-print correction. For crystal truncation rods, the angles vary in a more complicated way during the measurement and it is more convenient to multiply the data, rather than the model, by the following factors: the Lorentz correction with rod interception, $\sin\Phi\cos\alpha_i$, the linear polarization correction, $1/(1-(\sin\alpha_i\cos\Phi\cos\alpha_f + \cos\alpha_i\sin\alpha_f)^2)$, as well as footprint and active area corrections.

IV. RESULTS

A. Wetting Layer and the Transition to Islands

Grazing incidence diffraction was used to investigate the transition from the wetting layer phase to the formation of the islands as well as to investigate their epitaxial relationship with the Si(111)7x7. Fig. 3 shows the coverage dependence of the $(6/7,0)_H$ intensity, which comes from the Ag/Si(111)7x7 wetting layer, along with the Ag(2,1)_H intensity that corresponds to FCC Ag. The $(6/7,0)_H$ intensity changes with coverage as Ag is incorporated commensurately onto the Si(111)7x7 surface up until a coverage of ~ 0.4 ML where the intensity stops changing, although, the intensity does not vanish. Therefore the wetting layer structure saturates and completely wets the Si(111)7x7 surface near ~ 0.4 ML.

Extensive crystallographic evidence for the saturating wetting layer structure was obtained by measuring a series of many seventh-order diffraction intensities, $(H,K,0.1)_H$, as a function of coverage in 0.1 ML increments, as shown in Fig. 4 where each diffraction intensity is normalized by its value measured at 0.5 ML coverage. In order to allow for the time needed to measure the many seventh-order diffraction intensities, the deposition was

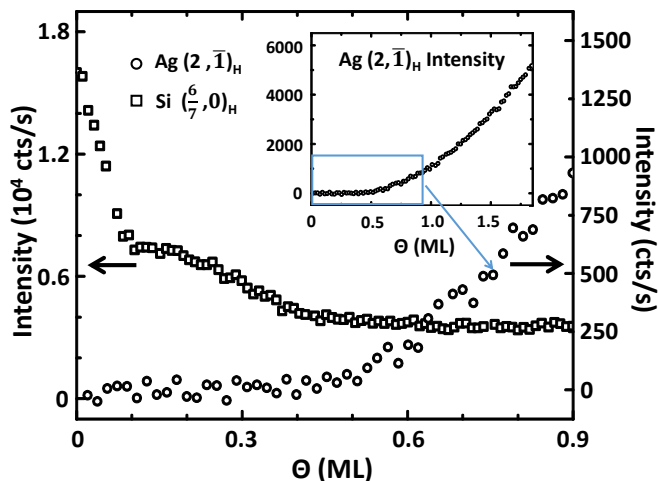


FIG. 3: $(6/7,0)_H$ and $Ag(2,\bar{1})_H$ intensity at $L=0.1$ as a function of Ag coverage during deposition at 360K and 300K, respectively. FCC Ag islands begin to form only after the wetting layer structure saturates.

performed at the usual flux rate but paused after each 0.1 ML was deposited, with the time between each deposition step being ~ 20 minutes. It can be seen that all of the intensities vary strongly, and in different ways, as Ag is incorporated commensurately into the $Ag/Si(111)7\times 7$ wetting layer structure. This intensity variation occurs up to a coverage of ~ 0.4 ML, above which there is negligible change in intensity. Therefore the $Ag/Si(111)7\times 7$ wetting layer neither changes its structure nor absorbs more Ag for a coverage above ~ 0.4 ML.

Ag FCC islands are observed to form above a coverage of 0.4 ML, as indicated by the onset of the $Ag(2,\bar{1})_H$ intensity in Fig. 3. Although this coverage is consistent with previous STM studies of $Ag/Si(111)7\times 7$ ^{21,22,25}, the x-ray scattering measurements are representative of the entire surface and they demonstrate, macroscopically, a sharp transition to the formation of islands after the complete saturation of the wetting layer. The x-ray scattering measurements additionally reveal that the islands are comprised of incommensurate FCC Ag having the bulk Ag lattice constant.

The orientational alignment of the islands relative to the substrate was investigated by performing a scan azimuthally at $L=0.1$ along a circle in the HK plane having the radius of $Ag(1,1)_H$ for bulk Ag, as shown in Fig. 5. The two large peaks are 60° apart and correspond to FCC Ag islands that are aligned along the substrate crystallographic axes such that the $Ag[1,1]_H$ and $Si[1,1]_H$ are parallel. Fig. 5 also shows weaker “satellite” peaks having an orientation $15.7 \pm 0.2^\circ$ on either side of the $\{1,1\}_H$ directions, revealing a smaller population (18%) of rotated islands. The azimuthal width of both the main peak and the satellites correspond to an orientational disorder (mosaicity) of $\sim 3.7^\circ$ in the plane of the surface; orientational fluctuations do not occur out of the surface plane. As was

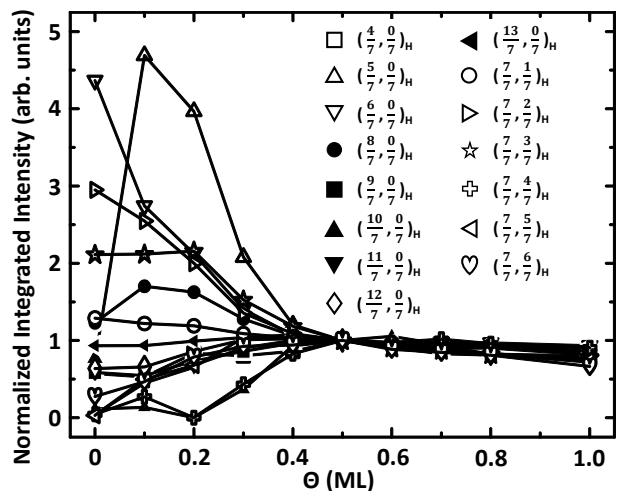


FIG. 4: Seventh-order diffraction intensities measured as a function of coverage at 360K. The intensity of each reflection is normalized by its value at 0.5 ML. All intensities exhibit a strong variation below 0.4 ML, indicating the development and evolution of the Ag wetting layer that is commensurate with the $Si(111)7\times 7$. This evolution does not occur above 0.4 ML as the Ag wetting layer structure completes and saturates.

previously noted²⁶, the commensurate Ag wetting layer is perfectly aligned orientationally with the $Si(111)7\times 7$, which has narrow ($\sim 0.03^\circ$) seventh-order peaks. We find that the seventh-order peaks do not broaden with Ag deposition, which indicates that as the wetting layer is formed the Ag decorates the $Si(111)7\times 7$ without reducing the original domain size of the reconstructed surface.

Fig. 6 shows that the main peak and the satellites exhibit the same radial position, indicating that the satellites are due to truly rotated islands rather than a superstructure: both populations of Ag islands are observed to have the conventional Ag lattice constant to within our resolution of $\pm 0.3\%$. Both peaks have the same radial width, which is slightly larger than the instrumental resolution, and it suggests an average lateral island size on the order of 300Å. The satellite peaks are also observed at the same rotation angle when Ag is deposited at temperatures lower than in Fig. 5, although, the satellite intensities are weaker. Therefore, the population of the rotated islands decreases with decreasing temperature, suggesting a kinetic barrier to their formation.

B. Vertical Structure and the Atomic Layer Morphology of the Islands

In order to establish the evolution of the vertical structure, we begin by analyzing the specular reflectivity at the lowest coverage where there are no islands, as shown in Fig. 7a for 0.3 ML of Ag deposited on $Si(111)7\times 7$ at 300K. Near $L=2.6$ there is a cusp in the reflectivity where its position and depth is sensitive to both the height z_{wet} and the coverage Θ of the wetting layer. Least-squares

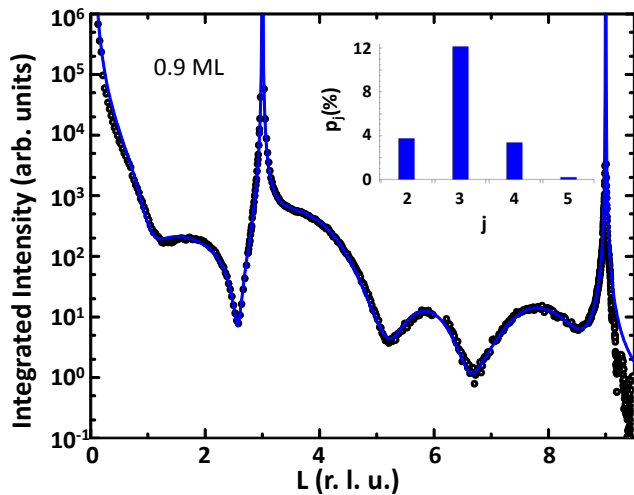


FIG. 8: Specularly reflected intensity measured for 0.9 ML Ag deposited on Si(111)7x7 at 300K. Solid curves are a best fit to the model described in the text. The inset shows the histogram of p_j where there are predominantly 3-layer islands.

Ag deposited at 300K, as shown in Fig. 7b. Compared with the measurement for 0.3 ML, the reflectivity clearly shows small but broad peaks around $L=3.98$ and 7.96 , which are the locations of the Ag(111) and Ag(222) Bragg reflections and, therefore, indicates the existence of FCC Ag islands. From our fit to the data, we find that $\sim 5\%$ of surface is covered by islands. It is noteworthy that the *first* emergence of islands at this lowest coverage shows the predominance of *three* atomic layers.

Measurements were also performed at higher coverages. Fig. 8 shows a specular reflectivity measurement for 0.9 ML Ag deposited on Si(111)7x7 at 300K where two FCC Ag Bragg peaks appear prominently near $L=3.98$ and 7.96 as well as one subsidiary maximum that is located between them. In analogy to a three-slit optical interference pattern and because the Ag dominates the scattering, the single subsidiary maximum in between the Bragg positions suggests islands having three atomic layers with the conventional lattice spacing of FCC Ag. Quantitatively fitting the data gives a height distribution shown in the inset, which indeed indicates the predominance of three-layer islands. Fig. 9 shows a specular reflectivity measurement for 1.8 ML Ag deposited on Si(111)7x7 at 300K. A fit to the data reveals the predominance of four-layer islands, which is qualitatively apparent from the two subsidiary maxima between the Bragg peaks. Among all of the fitted data we find that the RMS island position fluctuations (Eq. 6) are $\sigma = 0.1 \pm 0.05 \text{ \AA}$ and the accuracy of the height distributions, p_j , are about ± 0.01 . Finally, we find that for all coverages, the wetting layer and the islands exhibit the same distance above the substrate, $z_{wet} = z_{island}$ to within 0.15 \AA .

We now turn to the interfacial atomic layer of Ag that lies between the island and the substrate (the cross-hatched layer in Fig. 2), which was discussed in Ref.[26

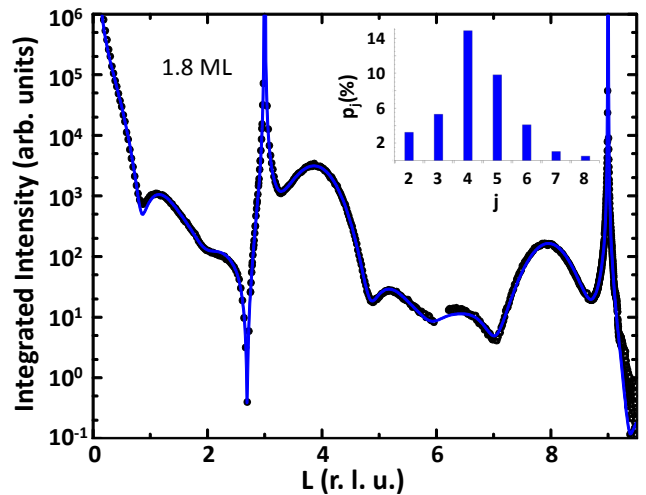


FIG. 9: Specularly reflected intensity measured for 1.8 ML Ag deposited on Si(111)7x7 at 300K. Solid curves are a best fit to the model described in the text. The inset shows the histogram of p_j where there are predominantly 4-layer islands at this higher coverage.

]. The viewpoint of a conventional Stranski-Krastanov (SK) growth mode has been consistently applied to metals grown on semiconductors where it is *assumed* that the islands are positioned *on top* of the wetting layer. However, Ref.[26] showed that situation does not occur for Ag/Si(111)7x7 where the FCC islands consume the wetting layer and the islands exist all the way to the substrate.

It is noted that x-ray reflectivity alone cannot make this determination because it is insensitive to the lateral atomic structure so that all layers contribute to the specular reflectivity, as can be seen from Fig. 1. Any difference between the wetting layer and the first FCC layer would have to be distinguished by a small difference in electron density. Therefore, it would be difficult to determine whether the first atomic layer is entirely wetting layer or whether it is a mixture of wetting layer and FCC Ag from the islands – the distinction would have to be made quantitatively, based only on the Ag density. The difficulty is compounded by the fact that the wetting layer and the islands exhibit identical vertical distances from the substrate. However, measuring a truncation rod of the FCC Ag in Fig. 1 will uniquely identify the FCC Ag contribution.

The specular reflectivity and the Ag(1,1)_H crystal truncation rod results are shown in Fig. 10a and Fig. 10b, respectively, and the island height distributions, p_j , obtained from these two sets of data are shown in Fig. 11. To make the comparison of the two height distributions, the p_j determined from the truncation rod was normalized so that it has the same $\sum_{j=2} p_j$ as that obtained from the specular reflectivity. This was necessary because, as noted in Sec. III, the reflectivity determines p_j absolutely whereas the rod leaves an unknown scale factor. The two height distributions are nearly identical

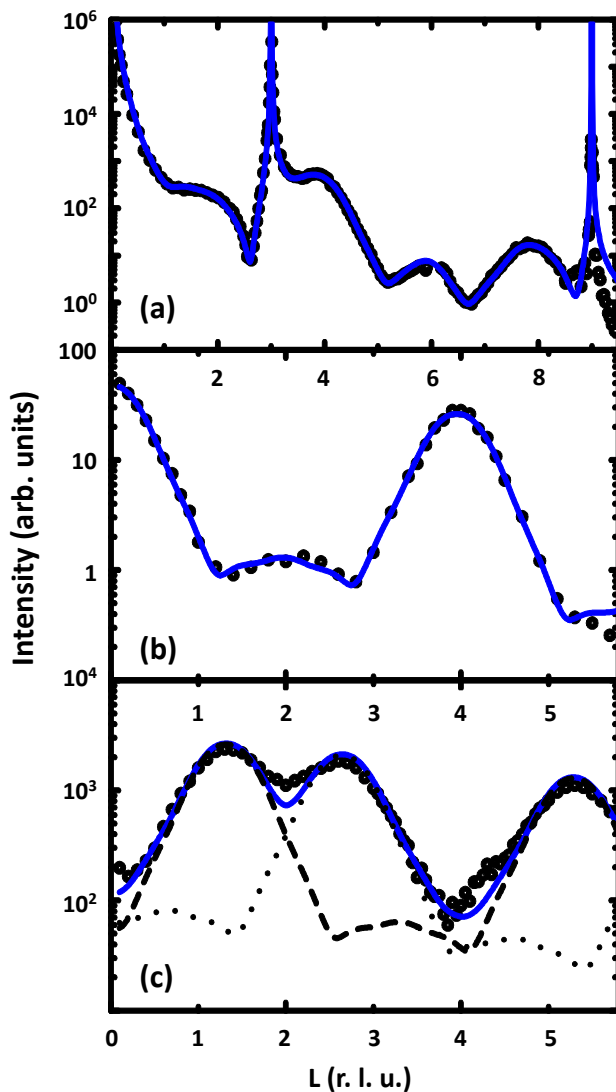


FIG. 10: Specular reflectivity and crystal truncation rod measurements from 0.9 ML Ag deposited on Si(111)7x7 at 360K. Solid curves are a best fit to the model described in the text. (a) Specular reflectivity and (b) Ag(1,1)_H rod measured with fixed incident angle. (a) and (b) are the same data and fitted curves as in Ref.[²⁶]. (c) Ag (1,0)_H rod measured with fixed exit angle. The dashed and dotted curves show the relative contributions of Ag(1,0)_H (dashed) and Ag(0,1)_H (dotted) rods that arise due to 60° rotated islands.

for p_2 and higher, indicating that the islands extend all the way to the substrate without an intervening wetting layer, as was concluded in Ref.[²⁶]. Of course, very different results for the first atomic layer are obtained from the truncation rod and the specular reflectivity because the latter is dominated by p_{wet} whereas the former is sensitive only to p_1 . Interestingly, there is a small but non-zero p_1 (2% coverage) from the truncation rod measurement, which we suggest might arise from a small amount of re-ordering of the commensurate wetting layer

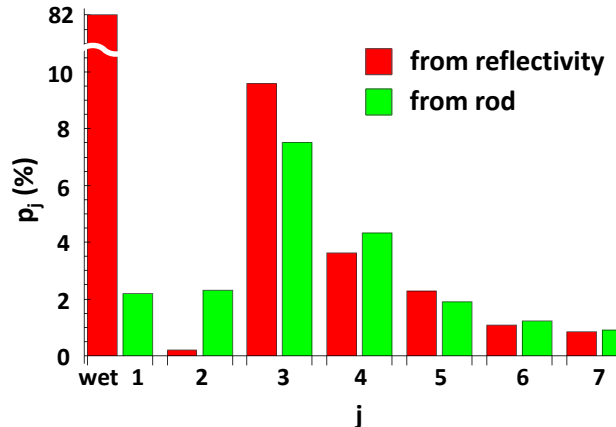


FIG. 11: Comparison of the island height distributions obtained from fits to the specular reflectivity (Fig. 10a) and the Ag(1,1)_H truncation rod (Fig. 10b). The left (right) column represents p_j obtained from reflectivity (truncation rod). As can be seen, the reflectivity and the truncation rod measurements give nearly identical island height distributions for $j \geq 2$, indicating that the FCC Ag islands extend to the substrate. The large difference between p_1 and p_{wet} arises from the way that the two measurements see the wetting layer and the FCC islands, as discussed in Sec. III. p_j for $j \geq 2$ are the same as in Ref.[²⁶].

into incommensurate Ag in the immediate proximity of the island, perhaps in the form of a narrow annular ring around the island.

A scan along another crystal truncation rod, the Ag(1,0)_H is shown in Fig. 10c. Unlike the Ag(1,1)_H rod, which is six-fold symmetric, the Ag(1,0)_H rod is three-fold symmetric with Bragg peaks expected at $L=1.328$ and $L=5.311$ ($L=1$ and 4 in Ag coordinates) along the rod. However, it can be seen that an additional peak is observed at $L=2.656$, which corresponds to the related, but inequivalent, Ag(0,1)_H rod. The fitted curve uses the p_j distribution obtained from the fit to the Ag(1,1)_H rod along with approximately equal contributions (1.08 to 1 ratio) of the Ag(1,0)_H and Ag(0,1)_H rods. Therefore, the Ag islands consist of 60° rotated domains, which is consistent with the nucleation of FCC islands on the six-fold symmetric Si(111)7x7.

Fig. 12 summarizes the coverage-dependence of the height distributions that were determined from our experiments at 300K. The vertical axis of the plot is the population of islands having a given height relative to the total population of the islands, $\frac{p_j}{\sum_{j=2} p_j}$. It can be seen that there is a clear preference for three-layer islands at low coverage; however, as the coverage increases, the preference shifts towards taller islands. Because prior STM studies have assumed that the islands grow on top of the wetting layer, it should be noted that our FCC Ag island heights are one monolayer thicker than those re-

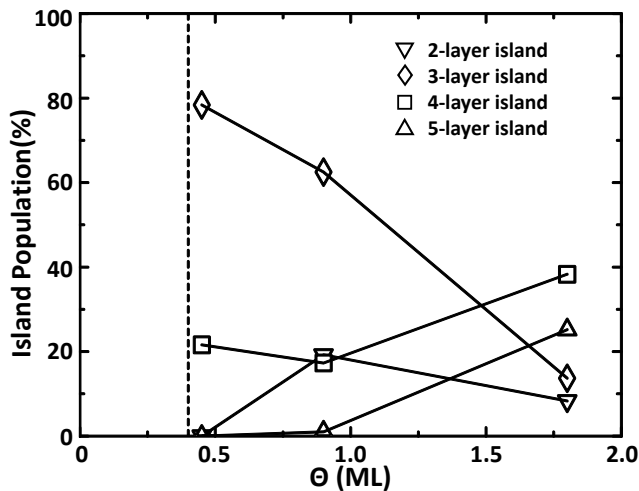


FIG. 12: Population, $\frac{p_j}{\sum_{j=2} p_j}$, of island heights measured as a function of Ag coverage at 300K. The vertical dashed line indicates the coverage at which islands begin to form after the completion of the wetting layer.

ported in the literature. Accounting for that difference, however, the island height distributions that we observe are in good agreement with prior STM work²⁵.

V. DISCUSSION AND CONCLUSIONS

In summary, our experiments investigate the atomic-scale interfacial structure during the growth and evolution of Ag on Si(111)7x7 over a range of coverage, beginning at the wetting layer and continuing through the formation of the islands. This x-ray scattering investigation presents an important new perspective on the structure and it complements what is known from recent STM studies. Below, we discuss our results in the order of coverage, from the wetting layer through island formation.

Our results provide new insight on the formation of the Ag/Si(111)7x7 wetting layer. Although the atomic-scale structure of the wetting layer is currently not known, STM studies have shown that Ag occupies half unit cells (HUCs) of the Si(111)7x7 which act as a template for the deposited Ag¹⁵⁻²⁰. There is a maximum occupancy of Ag in a HUC and, once a particular HUC is filled, further Ag atoms begin to fill a neighboring HUC^{18,19}. This scenario leads to a disordered network of Ag-filled HUCs that comprise the wetting layer^{17,22}. The coverage dependence of the surface diffraction intensities in Fig. 4 impose constraints on models that describe how Ag fills the HUCs. Each reflection in Fig. 4 is observed to have a different coverage dependence and some reflections exhibit extrema. This behavior of the intensities can be shown to be inconsistent with growth that proceeds by increasing the number of identical HUCs which are filled with Ag. Instead, the results of Fig. 4 indicate that the average crystallographic structure of the Ag-filled HUCs evolves

continuously with coverage until a significant fraction of the saturation coverage is attained. Our result is consistent with a recent STM study which showed that the number of HUCs containing Ag saturates very early in the growth (<0.1 ML) and these HUCs accumulate Ag continuously as more Ag is deposited²⁰.

From the reflectivity measured at low coverage in Fig. 7a, the Ag wetting layer is determined to consist of one atomic layer that sits at $z_{wet} \sim 2.2\text{\AA}$ above the Si-1a layer of the Si(111)7x7. This distance is only slightly larger than the height of the Si ad-atoms above Si-1a ($\sim 1.6\text{\AA}$ ²⁷), which implies that the Ag atoms in the wetting layer are located laterally between the Si ad-atoms *within* the Si ad-atom layer. This location of the Ag is consistent with low-temperature STM studies which have suggested that Ag adsorbs at high coordination sites between the Si ad-atoms in the case when only one or two Ag atoms occupy a HUC^{34,35}, although, in those studies the height was not determined.

Once the saturation coverage of the wetting layer is reached, our measurements in Fig. 4 reveal that the wetting layer no longer adds Ag or changes its crystallographic structure, which is remarkable given the discontinuous and disordered morphology of the wetting layer that contains a large amount of unoccupied HUCs. Even well above the coverage where islands form, the diffraction intensities change negligibly, with Fig. 4 showing only a slight intensity decrease of all 7-th order diffraction peaks from 0.5 to 1.0 ML. The small amount of the intensity decrease observed in Fig. 4 is approximately consistent with the $\sim 20\%$ Ag wetting layer loss due to island formation at 1 ML coverage, which is estimated from Fig. 11. STM measurements that tunnel through the islands have shown the presence of 7x7 symmetry beneath the island, although, the STM could not determine whether it came from the Si(111)7x7 or the Ag/Si(111)7x7 wetting layer²⁵. Our results demonstrate that the 7x7 symmetry beneath the islands is due to the Si and not the Ag wetting layer. The intensity decrease observed for all reflections, therefore, suggests that pristine Si(111)7x7 is not recovered: it is either disordered or a slightly different structure having 7x7 symmetry, possibly involving lateral displacements of the Si ad-atoms.

The onset of Ag island formation is observed near 0.4 ML, which was determined from both lateral and vertical structural measurements. The in-plane diffraction of Fig. 3 shows the formation of FCC Ag at the coverage where the wetting layer structure saturates. Vertically, the reflectivity in Fig. 7 shows that no islands are present at 0.3 ML and that the wetting layer is confined to one atomic layer of Ag, whereas at 0.45 ML islands can be detected in the reflectivity. It is emphasized that x-ray scattering provides an atomic-scale measurement that is an average over the macroscopic surface. Therefore, the saturation of the wetting layer concomitantly with the onset of islands suggests a macroscopic two-phase coexistence between islands and the wetting layer.

It is observed that there is both a coverage and tem-

perature dependence to the average island height. When islands form, the wetting layer below the island is dissolved so that the interfacial atomic layer of the islands is FCC Ag and the island height is measured from the interface with the substrate²⁶. As shown in Fig. 7 there is a minimum island height of three layers, even at extremely low coverage when only 5% of the surface is covered by islands. The predominance of trilayer islands continues to be observed at higher coverage (Fig. 8), although further increasing the coverage leads to an average island height greater than three layers, as shown in Fig. 9. It is also found that the average island height increases and the island height distribution broadens with increasing temperature, which results from increased kinetics²⁶. Therefore, the minimum island height is three atomic layers of FCC Ag, although, the islands can attain a taller height depending on the temperature and the coverage. Nevertheless, even with average island heights greater than three layers, it is shown elsewhere that the system manifests the three-layer minimum height in the temperature and coverage dependence³⁶.

Although it was reported that STM studies consistently find a significant vertical expansion of the Ag lattice²⁵, x-ray reflectivity and crystal truncation rods observe the conventional Ag lattice constant, as was discussed by Chen et al.²⁶. Here, we address this apparent discrepancy by suggesting that the STM is sensitive to important differences between the electronic properties of the islands and the Ag wetting layer. In particular, it is noted that the Ag wetting layer contains a low density of Ag, which likely leads to a smaller conductivity and tunneling efficiency into the wetting layer. That would require the STM tip to be closer to the wetting layer than when measuring near the top of the electronically denser islands, thereby leading to an apparent expansion of the Ag islands when their heights are measured by STM relative to the wetting layer position. Because x-rays scatter from all of the electrons in an atom, the x-ray scattering measurements are therefore sensitive to the actual atomic positions.

We now consider the orientational properties of the Ag islands in terms of their relationship to the substrate. Because the wetting layer completely and macroscopically forms before the Ag islands appear, the islands have a weaker interaction with the substrate than the wetting layer. This fact apparently enables orientational disorder (mosaicity) of the islands as well as a rotated orientation that is observed in Fig. 5. We do not observe the Ag(001)-normal orientation that has been reported on surfaces prepared at higher temperature on the $\text{Si}(111)\sqrt{3}\times\sqrt{3}\text{-R}30^\circ$ ^{37,38}. If this island orientation was present, it would have a significant impact on our measured island height distribution which was independently corroborated from both reflectivity and truncation rods, in Fig. 11. We observe only Ag(111)-normal orientated islands with most of the islands having the in-plane $\text{Ag}(1,1)_H$ oriented along $\text{Si}(1,1)_H$ along with a small population of islands rotated from this direction

by 15.7° . The two orientations and their mosaicity occur despite the fact that the Si and FCC Ag lattice constants are very close to a 4:3 ratio, differing by only 0.4%. The relationship between the bulk Si and the two Ag orientations is shown in Fig. 13. Because the buried interface of the FCC Ag islands is with $\text{Si}(111)7\times 7$ and not bulk $\text{Si}(111)$, geometrical constraints at the interface will be an important factor in generating the mosaicity and the island orientations, as discussed below. Similarly, we do not observe the 19° rotation that was found for Ag on $\text{Si}(111)\sqrt{3}\times\sqrt{3}\text{-R}30^\circ$ ³⁸, which is additional evidence that the structural details at the interface are important.

The Si ad-atoms should be considered for interpreting the epitaxial relation of the FCC Ag islands to the $\text{Si}(111)7\times 7$. The low height of z_{island} implies that the bottom interfacial atomic layer of the FCC Ag islands inhabits the relatively large open spaces in between the Si ad-atoms within the Si ad-atom layer of the $\text{Si}(111)7\times 7$. The areal density of FCC Ag would yield approximately 86 Ag atoms within a 7×7 unit cell whereas there are only 12 Si ad-atoms in this same area. Therefore, it is likely that the interfacial atomic layer of the FCC Ag islands contains defects, perhaps in the form of vacancies, in order to accommodate the Si ad-atoms. Although the interfacial atomic layer of the FCC Ag islands is mainly with the six-fold symmetric Si-1a layer that has both faulted and unfaulted halves with respect to the bulk structure, the protruding Si ad-atoms laterally reside above the bulk Si-1b positions and they might also play a role in the orientation of the Ag islands. In either case, using the bulk $\text{Si}(111)$ as a reference is a reasonable first step for investigating the orientation of the FCC Ag islands with respect to the substrate.

To investigate the rotation of the Ag islands, we first consider coincidence-site lattices³⁹ that have been previously used for metals on $\text{Si}(111)$ ^{38,40,41}. Here, we investigate rotated supercells of Ag that are nearly lattice-matched with Si supercells. By generating a list of possible coincidence lattices having supercells containing less than 100 Si atoms (176 Ag atoms) and accepting only those for which the ratio of the Si/Ag supercell lattice constants is the same to within 0.5%, we have found a 15.8° rotated coincidence lattice that is very close to the 15.7° rotation observed experimentally. Two nearby rotations of 14.4° and 16.6° are also found and they will be discussed below. The 15.8° rotated supercell is shown schematically in Fig. 13 in comparison to the bulk $\text{Si}(111)$. As can be seen, this supercell has an area that is similar to the area of the $\text{Si}(111)7\times 7$ unit cell, although the supercell is slightly smaller. The similar size to the $\text{Si}(111)7\times 7$ might, in part, explain why this particular coincidence lattice is favored by the system.

By examining the rotated Ag lattice in relation to its interface with the Si-1a layer of the $\text{Si}(111)7\times 7$, we can show that certain rotations lead to the clustering of coincident supercells into domains. Fig. 14 shows the points of coincidence of the Si-1a positions with the corners of the Ag supercells for four different rotation angles. It is

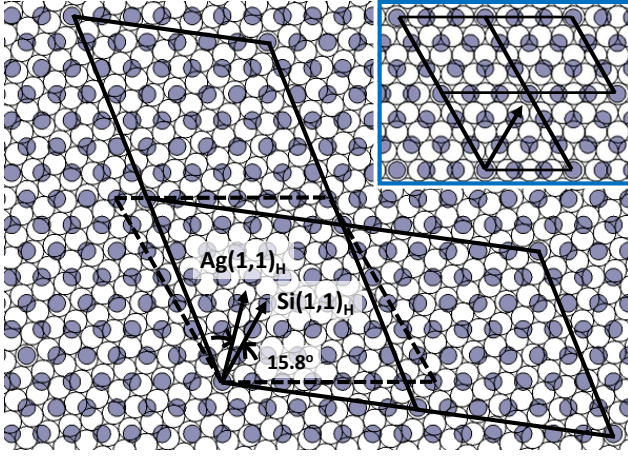


FIG. 13: Diagram showing the coincidence lattices of Si(111) and Ag(111), which have lattice constants in the ratio of 4:3. The open circles are Ag and the filled circles are Si. The solid line shows a coincidence lattice that is rotated by 15.8° , which closely matches the angle of the rotated domains observed in the measurements. The dashed line shows a Si(111) 7×7 cell. The inset shows the Si and Ag lattices without rotation, where the arrow is parallel to both the $\text{Ag}(1,1)_H$ and $\text{Si}(1,1)_H$ directions.

striking that relatively large clusters of coincident supercells are present for the unrotated and the 15.8° orientations, but not for the two nearby coincidence lattice rotations that we found at 14.4° and 16.6° . We suggest that the clusters of coincident supercells are necessary for the initial formation of the FCC Ag islands. In consideration of kinetic barriers, it is noted that the unrotated cell has the smallest area and it is therefore the easiest orientation to form whereas the larger area of the 15.8° cell would have a relatively higher kinetic barrier, which is consistent with experimental observation. As noted above, the Si ad-atoms follow the bulk Si positions and they would be consistent with any of the coincidence lattices determined relative to bulk Si. Therefore, these results suggest that the different symmetries of the faulted and unfaulted halves of the Si-1a layer of the Si(111) 7×7 surface play an important role in selecting the orientation of the FCC Ag islands.

A remaining question concerns why the islands consume the Ag wetting layer? Typically, Stranski-Krastanov growth results from an energy transition mechanism at the interface where a wetting layer is preferred and followed by the growth of islands. Although that situation is relevant in the present case, growing on top of the Ag wetting layer presents a problem. Given the discontinuous morphology of the Ag wetting layer, islands formed on top of the wetting layer would be energetically expensive for a rough buried interface. One would not have flat-topped Ag islands if they conformed to such a rough wetting layer. Consequently, removing the wetting layer in the region of the FCC Ag is-

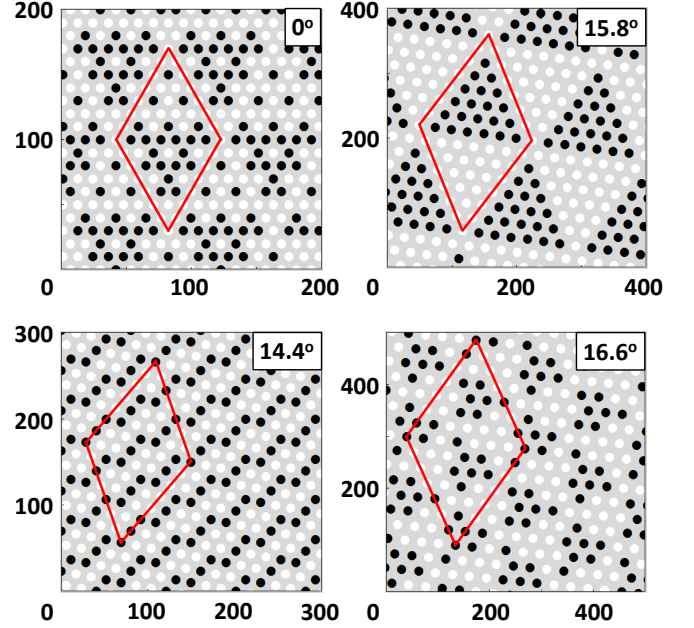


FIG. 14: The coincidence of Ag supercells with the Si-1a layer are shown for different rotations: unrotated supercell containing 16 Ag atoms; 14.4° rotated supercell containing 37 Ag atoms; 15.8° rotated supercell containing 76 Ag atoms; and 16.6° rotated supercell containing 129 Ag atoms. All circles represent the corners of the Ag supercells and the filled circles show where the Ag supercells are coincident with the Si-1a atomic positions. The numeric scale on the axes is given in units of Angstroms. The solid lines outline periodic domains that result from the Ag coincidence lattice superimposed on the 7×7 period. It can be seen that significant clusters of coincident supercells occur for 0° and 15.8° rotations but not for 14.4° and 16.6° .

lands seems plausible given the discontinuous wetting layer morphology. A similar situation where the wetting layer is dissolved by islands was reported for Pb on Si(111) 7×7 ^{42,43}, although, the Pb system differs from Ag in that it exhibits a dense and *continuous* wetting layer morphology. However, the Pb wetting layer has a large vertical disorder or corrugation⁴³ so that Ag and Pb are similar in the sense that they both have a rough wetting layer which would lead to an energetically unfavorable interface between the island and the wetting layer. The fact that the Pb islands consume the wetting layer in Pb/Si(111) 7×7 was determined from the relative roughness of the wetting layer as compared to the islands⁴³ and from the vertical displacement that the islands experience relative to the wetting layer⁴² – the latter effect does not occur for Ag/Si(111) 7×7 . By comparison, the Ag/Si(111) 7×7 system more directly lends evidence for islands consuming the wetting layer because of the uniform Ag island heights which enable the combined use of specular reflectivity and crystal truncation rods.

The energetic condition that leads to a locally dissolving wetting layer is related to the interfacial energy per

area for the island on the substrate, γ_I , the wetting layer on the substrate, γ_W , the island on the wetting layer, γ'_I , and the wetting layer on the substrate but with the island on it, γ'_W . Consideration of these leads to the condition: $0 < \gamma_I - \gamma_W < \gamma'_I + (\gamma'_W - \gamma_W)$ where the left inequality is the requirement that the wetting layer rather than the islands initially form on the substrate and the right inequality is the condition for the islands to dissolve the wetting layer rather than form on top of the wetting layer.

In conclusion, important new structural information on the Ag wetting layer and the islands have been obtained using in situ x-ray scattering, which is a unique tool to investigate the buried interfaces of nanostructures. Future work is needed to better understand the crystallographic structure of the wetting layer. An important remaining question is why the saturated discon-

tinuous wetting layer stops accepting Ag even though there is physical space in the unoccupied HUCs. Also, new in situ x-ray scattering studies of other heteroepitaxial systems are needed in order to gain a comprehensive understanding of the evolution of the buried interfaces during SK growth.

VI. ACKNOWLEDGMENTS

Support from the National Science Foundation under grants DMR-0706278 and DGE-1069091 is gratefully acknowledged. The Advanced Photon Source Sector 6 beam-line at Argonne National Laboratory is supported by the US-DOE under Contract No. W-31-109-Eng-38.

-
- ¹ R. T. Tung, Appl. Phys. Rev. **1**, 011304 (2014).
² P. Fan, U. K. Chettiar, L. Cao, F. Afshinmanesh, N. Engheta, and M. L. Brongersma, Nat. Photon. **6**, 380 (2012).
³ Y.-J. Lu, J. Kim, H.-Y. Chen, C. Wu, N. Dabidian, C. E. Sanders, C.-Y. Wang, M.-Y. Lu, B.-H. Li, X. Qiu, et al., Science **337**, 450 (2012).
⁴ A. R. Smith, K.-J. Chao, Q. Niu, and C.-K. Shih, Science **273**, 226 (1996).
⁵ Z. Zhang, Q. Niu, and C.-K. Shih, Phys. Rev. Lett. **80**, 5381 (1998).
⁶ Z. Suo and Z. Zhang, Phys. Rev. B **58**, 5116 (1998).
⁷ F. K. Schulte, Surf. Sci. **55**, 427 (1976).
⁸ M. Ozer, C.-Z. Wang, Z. Zhang, and H. Weiering, J. Low Temp. Phys. **157**, 221 (2009).
⁹ W. B. Su, C. S. Chang, and T. T. Tien, J. Phys. D **43**, 013001 (2010).
¹⁰ M. C. Tringides, M. Jaochowski, and E. Bauer, Phys. Today **60**, 50 (2007).
¹¹ K. Budde, E. Abram, V. Yeh, and M. C. Tringides, Phys. Rev. B **61**, R10602 (2000).
¹² M. Hupalo, S. Kremmer, V. Yeh, L. Berbil-Bautista, E. Abram, and M. C. Tringides, Surf. Sci. **493**, 526 (2001).
¹³ C. A. Jeffrey, E. H. Conrad, R. Feng, M. Hupalo, C. Kim, P. J. Ryan, P. F. Miceli, and M. C. Tringides, Phys. Rev. Lett. **96**, 106105 (2006).
¹⁴ A. Gray, Y. Liu, H. Hong, and T. C. Chiang, Phys. Rev. B **87**, 195415 (2013).
¹⁵ S. Tosch and H. Neddermeyer, Phys. Rev. Lett. **61**, 349 (1988).
¹⁶ G. Meyer and K. H. Rieder, Appl. Phys. Lett. **64**, 3560 (1994).
¹⁷ I. Ost'adal, P. Sobotik, J. Myslivecek, and T. Jarolimek, Czech. J. Phys. **49**, 1613 (1999).
¹⁸ P. Kocan, P. Sobotik, I. Ost'adal, and M. Kotrla, Phys. Rev. B **69**, 165409 (2004).
¹⁹ I. Ost'adal, P. Kocan, P. Sobotik, and J. Pudl, Phys. Rev. Lett. **95**, 146101 (2005).
²⁰ F. Ming, K. Wang, X. Zhang, J. Liu, A. Zhao, J. Yang, and X. Xiao, J. Phys. Chem. C **115**, 3847 (2011).
²¹ L. Gavioli, K. R. Kimberlin, M. C. Tringides, J. F. Wenzel, and Z. Zhang, Phys. Rev. Lett. **82**, 129 (1999).
²² P. Sobotik, I. Ost'adal, J. Myslivecek, T. Jarolimek, and F. Lavicky, Surf. Sci. **482-485**, 797 (2001).
²³ W. B. Su, H. Y. Lin, Y. P. Chiu, H. T. Shih, T. Y. Fu, Y. W. Chen, C. S. Chang, and T. T. Tsong, Phys. Rev. B **71**, 073304 (2005).
²⁴ D. K. Goswami, K. Bhattacharjee, B. Satpati, S. Roy, P. V. Satyam, and B. N. Dev, Surf. Sci. **601**, 603 (2007).
²⁵ B. Unal, A. Belianinov, P. A. Thiel, and M. C. Tringides, Phys. Rev. B **81**, 085411 (2010).
²⁶ Y. Chen, M. W. Gramlich, S. T. Hayden, and P. F. Miceli, Phys. Rev. Lett. **114**, 035501 (2015).
²⁷ I. K. Robinson and E. Vlieg, Surf. Sci. **261**, 123 (1992).
²⁸ B. D. Cullity, *Elements of X-Ray Diffraction (2nd Edition)* (Addison-Wesley Longman, Inc, 1978).
²⁹ W. C. Elliott, P. F. Miceli, T. Tse, and P. W. Stephens, Phys. B **221**, 65 (1996); P. F. Miceli, *Semiconductor Interfaces, Microstructures and Devices: Properties and Applications Chapter 4* (IOP publishing, 1993).
³⁰ K. Takayanagi, Y. Tanishiro, S. Takahashi, and M. Takahashi, Surf. Sci. **164**, 367 (1985).
³¹ E. Vlieg, J. Appl. Crystallogr. **30**, 532 (1997).
³² R. Feidenhans'l, Surf. Sci. Rep. **10**, 105 (1989).
³³ R. D. Aburano, H. Hong, J. M. Roesler, K. Chung, D. S. Lin, P. Zschack, H. Chen, and T. C. Chiang, Phys. Rev. B **52**, 1839 (1995).
³⁴ C. Zhang, G. Chen, K. Wang, H. Yang, T. Su, C. T. Chan, M. M. T. Loy, and X. Xiao, Phys. Rev. Lett. **94**, 176104 (2005).
³⁵ S. Hu, A. Zhao, E. Kan, X. Cui, X. Zhang, F. Ming, Q. Fu, H. Xiang, J. Yang, and X. Xiao, Phys. Rev. B **81**, 115458 (2010).
³⁶ Y. Chen, M. W. Gramlich, S. T. Hayden, and P. F. Miceli, manuscript in preparation.
³⁷ Y. Fujikawa, T. Sakurai, and R. M. Tromp, Phys. Rev. Lett. **100**, 126803 (2008).
³⁸ D. Wall, S. Tikhonov, S. Sindermann, D. Spoddig, C. Hassel, M. H.-v. Hoegen, and F. J. M. z. Heringdorf, IBM J. Res. Dev. **55**, 9:1 (2011).
³⁹ D. M. Hwang, T. S. Ravi, R. Ramesh, S.-W. Chan, C. Y. Chen, L. Nazar, X. D. Wu, A. Inam, and T. Venkatesan, Appl. Phys. Lett. **57**, 1690 (1990).

- ⁴⁰ H. H. Weitering, D. R. Heslinga, and T. Hibma, *Phys. Rev. B* **45**, 5991 (1992).
- ⁴¹ M. Yakes and M. C. Tringides, *J. Phys. Chem. A* **115**, 7096 (2011).
- ⁴² C. A. Jeffrey, R. Feng, E. H. Conrad, P. F. Miceli, C. Kim, M. Hupalo, M. C. Tringides, and P. J. Ryan, *Superlattices Microst.* **41**, 168 (2007).
- ⁴³ R. Feng, E. H. Conrad, M. C. Tringides, C. Kim, and P. F. Miceli, *Appl. Phys. Lett.* **85**, 3866 (2004).